CONCRETE RESEARCH LETTERS
www.crl.issres.net Vol. 4 (4) – Dec. 2013

Sample preparation technique on interfacial transition zone of steel fiber reinforced mortar

Siaw Foon Lee[1,*], Hilde Lea Lein[3] and Stefan Jacobsen[2]
[1] *CSIC, Eduardo Torroja Institute for Construction Science,28033Madrid, SPAIN*
[2] *Department of Structural Engineering, Norwegian University of Science and Technology (NTNU), NO-7491 Trondheim, NORWAY*
[3] *Department of Materials Science and Engineering, Norwegian University of Science and Technology (NTNU), NO-7491 Trondheim, NORWAY*

Received: 15/09/2013 – Revised 30/10/2013 – Accepted 20/11/2013

Abstract

A grinding and polishing procedure for steel fiber-reinforced mortar with a total time of 15 minutes and an average final surface roughness less than 1 μm is presented in this paper. This technique is performed on 3 different types of steel fiber-reinforced mortars, which are at w/b 0.3, with 0 and 10% silica fume and at w/b 0.5 with 0% silica fume. The samples prepared were then used for quantifying the interfacial properties at the region close to steel fiber using the backscattered electron image analysis and the nanoindentation. It reveals that the interfacial transition zone of steel fiber that has a diameter of 0.16 mm is around 30 μm. Steel fiber-reinforced mortars at w/b 0.3 with 0 and 10% silica fume have similar area % of porosity in the interfacial transition zone. However, according to a hardness profile, steel fiber-reinforced mortars at w/b 0.3 with 0% silica fume have better bonding in the interfacial transition zone compared to that with 10% silica fume.

Keywords: steel fiber-reinforced mortar; atomic force microscopy; interfacial transition zone; backscattered electron image analysis; nanoindentation

1. Introduction

Sample preparation for cementitious material such as cement paste, mortar and concrete has always been reported as a tedious task, mainly due to the presence of different phases, such as cement hydrates, aggregates, etc. in the cementitious material [1]. Although this work has been carried out quite often in the past, the previous publications only outlined the procedure without giving thorough and detail information about the criterion and the final surface roughness [2–7]. Therefore, new researchers who like to investigate into the micro-or nano-mechanical properties of cementitious using the backscattered electron image analysis and the nanoindentation technique find this task very time-consuming, especially in searching for the right equipment. Until lately, some researchers started to show the final surface roughness of the specimen and the equipment adopted in their laboratory [6] without detailed explanation about the procedure adopted. Table 1 shows the summary of the grinding and polishing procedure taken from the literature.

Table 1: The conditions of the grinding and polishing adopted in the literature

Material	Grinding	Polishing	Surface finish	Machine	Ref.
cement paste and mortar	-	-Dry-polished with silicon carbide grits from 30 to 4 μm. -Finished with a 1-μm impregnated diamond cloth with oil-based lubricant. -Sample is ultrasonically cleaned in alcohol.	-	-	[2]
cement paste	-Ground on diamond discs of 30 μm and 15 μm. -Ethanol is used as lubricant. -Sample is ultrasonically cleaned in ethanol	-Polished with MD-Plan 6 μm, MD-Plan 3 μm, MD-Dur 1 μm and MD-Dur 0.25 μm in ethanol/diamond grit polishing suspension. -Each polishing time: 2-4 min. -Sample is ultrasonically cleaned in ethanol.	-	At a low rotation speed and a moderate force	[3]
mortar	-Silicon carbide paper: grit size 120, 220, 500, 1000 and 1200. -Dry ground.	-Polishing cloths with diamond abrasives (9, 6, 3, 1 and 0.25 μm) with a non-aqueous lubricant. -Each polishing time: ~5min. -Sample is ultrasonically clean in acetone.	-	70 rpm and 7 N force	[4]
cement paste	-	Polishing with silicon carbide paper 6.5 μm), then polishing with diamond suspension 0.1 μm).	-	-	[5]
cement paste	-Ground on 120 grit ZirMet (Buechler) abrasive paper. -total grinding time: until the entire surface has been ground. -Sample is ultrasonically cleaned in n-decane for 5 min.	-A TexMet P (Buehler) pad with approximately 5 mL of 1 μm oil-based diamond suspension. -total polishing time: 8 hours. -Sample is ultrasonically cleaned in n-decane for 5 min.	-Inspection of clean surface by naked eyes reveals a mirror-like finish that reflects overhead light. -Using AFM, the RMS roughness is 52.9±35nm (maximum value)	-	[6]
PVA fiber-reinforced mortar	-1200 grit grinding paper (LECO Corp.). -30 s per step. -Sample is rinsed in water and immediately dried.	-Polishing with diamond solution (15, 9, 6, 3, 1 and 0.5 μm). -30 s per step. -Sample is rinsed in ethanol and allowed to dry.	-	150 rpm and 15 N force	[7]

With the development of technology, computer simulation in molecular scale in the field of nanoindentation and nanotribology on nanomechanical properties of metal is made possible [8]. This simulation technique could possibly be applied to cementitious materials. Thus, this would allow the comparison of load-displacement between simulation data and the experimental data [9] of cementitious material. However, if the good surface roughness is unable to achieve this will make the comparison becomes difficult. Furthermore, an ISO standard on nanoindentation states

that surface finish has a significant influence on the test results [10].

In order to change the intrinsic properties of cementitous materials from brittle to ductile, steel fibers have widely been incorporated into the mortar and concrete lately. Research has shown that due to the ability of steel fibers in bridging over the cement pastes, steel fiber-reinforced cementitious materials manage to show a ductile behavior during fracture mechanism like those of polymeric materials [11, 12].

However, the incorporation of steel fiber adds one more phase to the cementitious materials. Since steel fiber is ductile compared to cement paste which is brittle, this makes the grinding and polishing becoming difficult at the ITZ between steel fiber and cement paste.

Basically, there are four steps in the sample preparation of cementitious materials: 1) resin embedding, 2) grinding, 3) epoxy vacuum impregnation, 4) polishing. For the nanoindentation test, the step of epoxy vacuum impregnation is omitted. The purpose of vacuum impregnation of epoxy into the pores of cementitious materials is to make the pores appear as black color during the backscattered electron image analysis.

Due to the fact that until now no researcher has published about the sample preparation of mortar incorporated with steel fiber, this paper presents in detail the procedure used to prepare the mortar at w/b 0.3 and 0.5 incorporated with steel fiber. The countermeasures taken and the final surface roughness of steel fiber-reinforced mortar at w/b 0.3 and 0.5 due to this technique were discussed.

The samples with final surface roughness obtained from this technique were then used for the study of interfacial properties between the steel fiber and the bulk paste using the backscattered electron image analysis and the nanoindentation.

2. Experimental procedures

2.1. Materials

Three steel fiber-reinforced mortars with (a) w/b 0.3, 0% silica fume, (b) w/b 0.3, 10% silica fume, and (c) w/b 0.5, 0% silica fume were made. 0.3 vol% straight high carbon steel fiber with the length of 13 mm and the diameter of 0.16 mm was incorporated into the mortars. The binder here refers to the summation of cement and silica fume.

The materials used were Norcem Anlegg cement (an Ordinary Portland cement in Norway), water, limestone, superplasticizer (polycarboxylate polymers), sand 0-2 mm, sand 0-4 mm and steel fiber. The materials were measured in kg/m^3. 2 vol% air voids was assumed in the mix proportion.

The mix proportion of materials was in the ratio of 1:0.3:0:0.087:0.02:0.455:2.577:0.045 for mortar (a) w/c 0.3, 0% silica fume, 1:0.33:0.1:0.098:0.025:0.51:2.893:0.048 for mortar (b) w/c 0.3, 10% silica fume, and 1:0.5:0:0.115:0.012:0.6:3.4:0.057 for mortar (c) w/c 0.5, 0% silica fume.

The following procedures were used to mix the materials: 1) Sands, cement, limestone powder and silica fume were poured one after another into a 10-litre flat-bottomed mixer with a counter current paddle and blended for 1 minute at low speed. 2) With the mixer still running, simultaneously, water and superplasticizer were added slowly into the mixture in the duration of around 30 seconds. Steel fibers were then added in.

The mixer continued running for 4 minutes before stopped. 3) The mixture was left to set for 5 minutes. Any powder that stuck on the wall of the mixer was spaded down into the mixture. 4) The mixture was then blended for another 1 minute. The total mixing time is 11 minutes.

2.2 Initial preparation -resin embedding

After 28-day curing in water, small cube was cut from the center of the mortar using a low-speed diamond saw, being splashed with water during cutting. The small cubes were cleaned from contamination and then dried at 20℃ and 50% RH. A Struers TegraPol-31 grinding and polishing machine with an adjustable rotational speed and polishing pressure, together with a specimen holder of 160 mm diameter with six mounts of 25 mm diameter were used, see Figure1. The dimension of the cube was determined in such a way that its surface area was around 50% of that of the mounting cup [13]. In our study, the cube dimension was around 16 x 16 x 16 mm, which formed a surface area of around 52% of the mount area, see Figure 2.

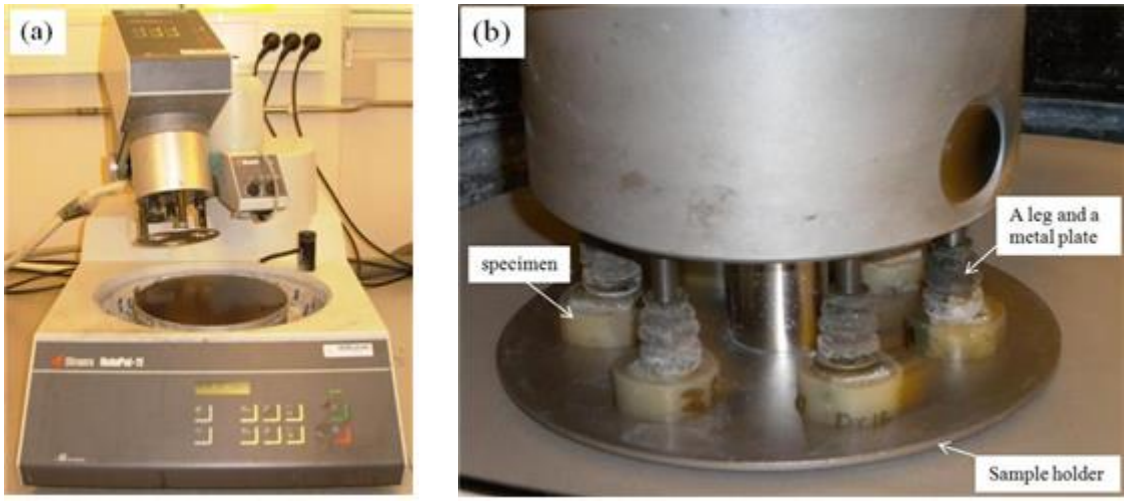

Figure 1. (a) The Struers TegraPol-31 grinding and polishing machine with (b) its sample holder.

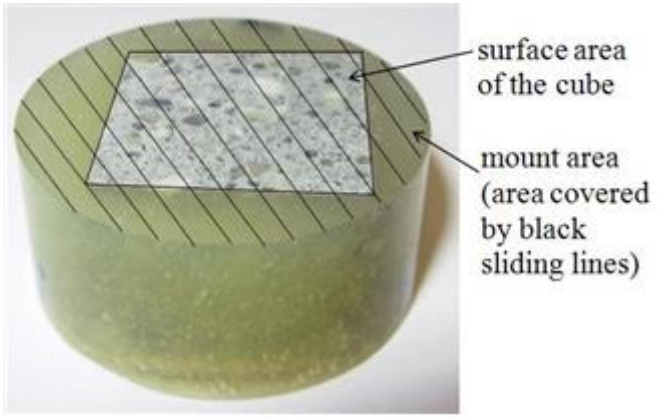

Figure 2. Specimen for grinding and polishing.

For easy handling during grinding and polishing, the cube was cold-mounted into epoxy resin in the mounting cup. The examined surface of the cube was put face down in a 25 mm diameter mounting cup. Araldite Standard Epoxy resin with bas and hardener in ratio 1:1 were blended well and then poured into the mounting cup. The epoxy together with the cube in the mounting cup was cured at 20℃ (a room temperature) for at least 24 hours. In the case that the cube is light and will float before the epoxy achieves full hardening, it is advisable to clamp the specimen at the side of a metal/table, see Figure 3. In this case, the examined surface will lay flat in

the mounting cup.

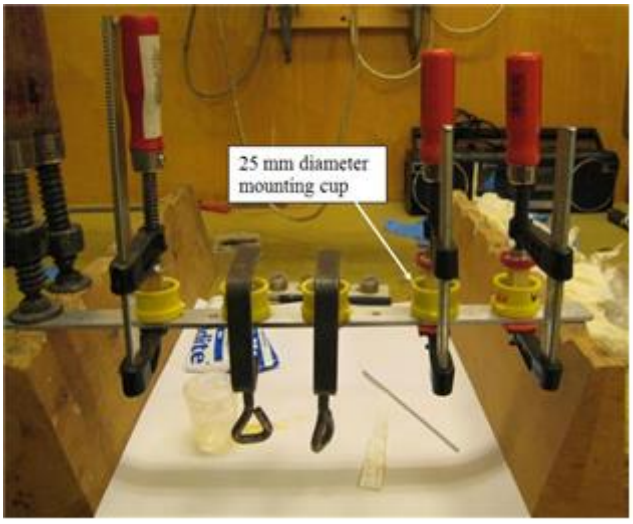

Figure 3. Specimens are clamped at the edge of a metal.

2.3. Grinding

Firstly, the base of the specimen was dry ground by hand for a few minutes on a Struers Silicon Carbide MD-Piano 600 that gave a 30 μm final surface flatness. The purpose was to ensure that the base of the specimen was flat. On the examined surface of the specimen, there exists a layer of epoxy that was very difficult to be noticed by naked eyes. However, this layer of epoxy became noticeable when it was viewed in a reflected light microscope at x10x10 magnification; see Figure 4 for its surface texture.

Therefore, it is necessary to grind the examined surface on MD-Piano 220 for a few times to get rid of the epoxy layer.

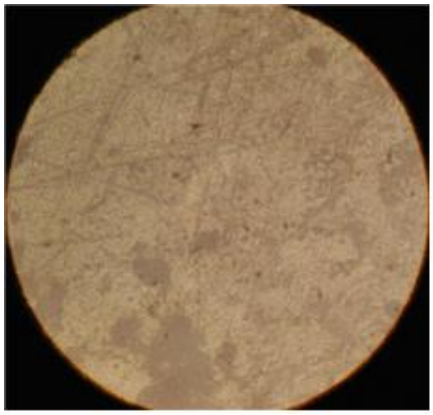

Figure 4. The surface texture of a specimen after the epoxy cold-mounting under a reflected light microscope at x10 x10 magnification.

In this study, the examined surface of specimen was ground using Struers Silicon Carbide MD-Piano 220 (68 μm), MD-Piano 600 (30 μm), MD-Piano 1200 (14 μm) and MD-Largo (9 μm) at a speed of 150 rpm. See Table 2 for the lubricant/abrasive, force and the duration adopted in this study. The specimen was cleaned ultrasonically in ethanol for about 2 minutes to remove grit and debris, and then it was examined in a reflected light microscope to check the effectiveness of each

step or any artifacts occurred.

Table 2: Grinding discs, polishing cloths, lubricant/abrasive, force and duration used for grinding and polishing specimens in this study

1) MD-Grinding Disc	**Lubricant/Abrasive**	**Force (N)**	**Duration (min)**
MD-Piano 220 (68 μm diamond)	Water	20	2
MD-Piano 600 (30 μm diamond)	Water	20	2
MD-Piano 1299 (14 μm diamond)	Water	20	2
MD-Largo	Ethanol/9 μm diamond grit suspensions	15	2
2) MD-Polishing Cloths			
MD-Plan	Blue Ethanol/6 μm diamond grit spray	10	2
MD-Dur	Ethanol/3 μm diamond grit suspensions	10	2
MD-Dac	Ethanol/1 μm diamond grit suspensions	10	2
MD-Nap	Blue Ethanol/¼ μm diamond grit spray	10	1

Figure 5 shows the images of the surface texture of specimen after each grinding under a reflected light microscope. Rough scratches could be seen on the steel fiber after the grinding using MD-Piano 220 (68 μm). The scratches became finer and finer when the grit number of MD-Piano disc increased. Debris of steel fiber could be seen attaching to the edge of steel fiber after the grinding using MD-Piano 1200 (14 μm), see Figure 5(c).

The attached debris of steel fiber disappeared after the grinding using MD-Largo (9 μm). At this stage, steel fibers showed fine circumferences for epoxy vacuum impregnation that would be carried out in the next step. If the attached debris of steel fiber was not removed, it would affect the study of the area % of the porosity in the ITZ.

2.4. Epoxy vacuum impregnation

The specimens were dried in a ventilated oven at 30℃ for 2 days before epoxy vacuum impregnation. The thickness of the specimen before and after epoxy impregnation was measured using a high-precision caliper. The purpose was to control the amount of the excessive epoxy that should be removed from the specimen surface before polishing.

The low-viscosity Epo-tek epoxy 301 and Epo-tek hardener were adopted. They were mixed in a ratio of 4:1 in a small bottle. The specimen with its examined surface facing up and the bottle with epoxy were put in the vacuum chamber pumped down to 40 mbar. This sucked out the entrapped air in the epoxy prior to impregnation. The bottle with epoxy was held by a clamp and it could be rotated freely using a handle outside the vacuum chamber.

The epoxy was poured slowly onto the top of the specimen to fully cover the whole surface. The epoxy on the examined surface of the specimen was set for about 10 minutes in the vacuum chamber before air was let gradually in to push it down into the specimen. The specimen was then cured in a temperature chamber at 40℃ at atmospheric pressure for at least 24 hours in order to achieve full bond strength.

The excessive epoxy was removed using a diamond surface grinding wheel until about 20-μm thickness of epoxy remains on the top of the specimen. The specimen was then hand ground with MD-piano 1200, at low rotation speed 150 rpm with water as lubricant, until its thickness

became about the same as the thickness measured before epoxy impregnation. The specimen was cleaned ultrasonically in ethanol for around 2 minutes after each grinding to remove the grit and debris.

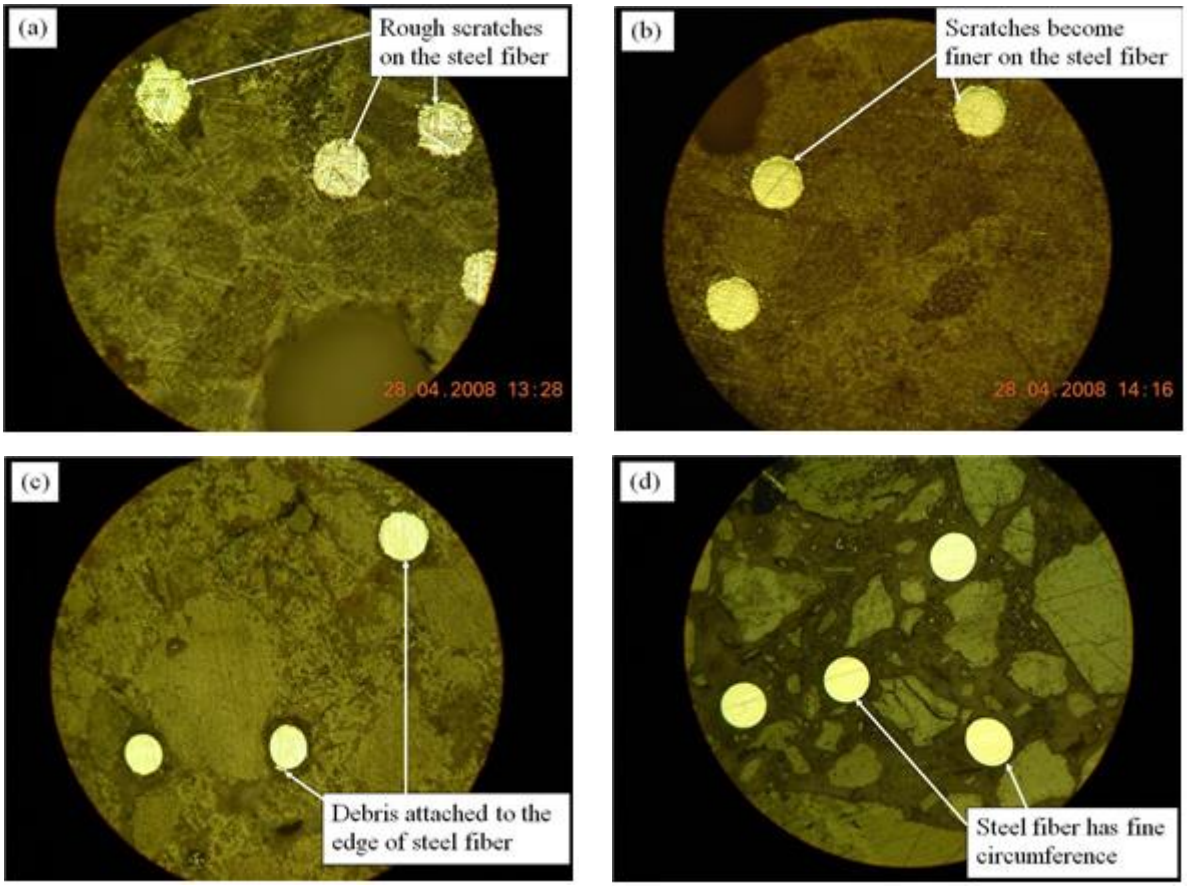

Figure 5. The surface texture of steel fiber, paste and aggregate under a reflected light microscope at x10 x10 magnification after each grinding using (a) MD-Piano 220 (68 μm), (b) MD-Piano 600 (30 μm), (c) MD-Piano 1200 (14 μm), and (d) MD-Largo (9 μm).

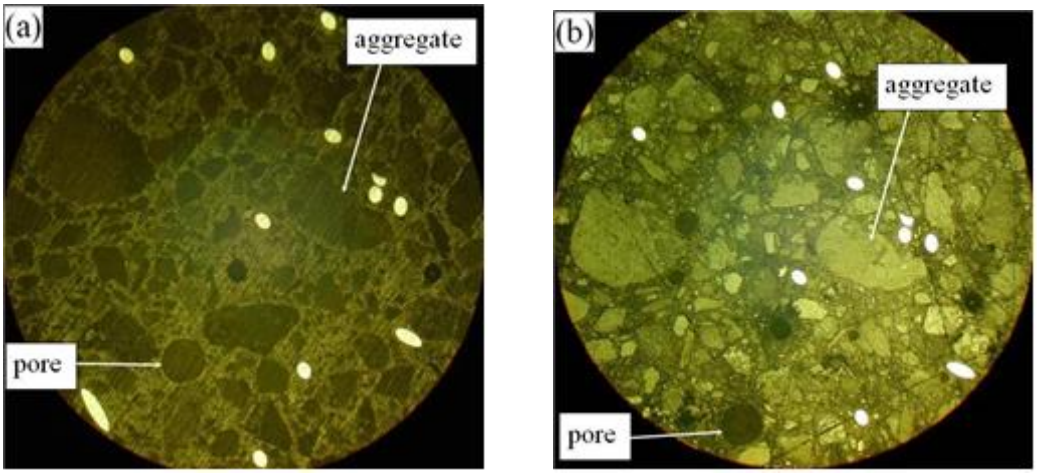

Figure 6. Images taken at x10 x2.5 magnification in a reflected light microscope. (a) Aggregates and pores appear homogeneous in color after epoxy vacuum impregnation. (b) Aggregates and pores appear inhomogeneous in color after a thin layer of epoxy has completely been removed.

2.5. Polishing

Figure 6 shows the surface texture of the specimen after epoxy vacuum impregnation in a reflected light microscope. When the surface was still coated with a layer of epoxy, aggregates and pores appeared homogeneous in color. MD-Largo (9 μm) disc was used to remove the layer of epoxy. After the thin layer of epoxy was removed, aggregates and pores appeared inhomogeneous in color. Great care needs to be taken for not polishing too much until below the epoxy intrusion depth [3]. After that, the examined surface of specimen was subjected to polishing.

The polishing cloths adopted were MD-Largo (9 μm), MD-Plan (6 μm), MD-Dur (3 μm), MD-Dac (1 μm) and MD-Nap (1/4 μm). The examined surface was polished at the low rotation speed of 150 rpm. The lubricant/abrasive, force and the duration used were indicated in Table 2. After each polishing, the specimen was cleaned ultrasonically in ethanol for around 2 minutes to remove the grit and debris. The examined surface was viewed in a reflected light microscope after each polishing to check the effectiveness of each step or any artifacts occurred. Figure 7 shows the surface texture of the examined surface of specimen after each polishing. At the final stage, the surface of steel fiber or aggregate appeared shining or flat in the reflected light microscope.

2.6. Atomic force microscopy

The surface roughness of specimen after final polishing was measured using the Nanosurf EasyScan2 atomic force microscope with Z resolution of 0.21 nm and X, Y resolution of 1.1 nm in tapping mode. The scanned area was 70 x 70 μm. The roughness average, the root mean square and the peak-valley height of the surface of steel fiber, steel fiber-ITZ, bulk paste and aggregate were measured. The measurements were generated from the program using the following equations.

The roughness average, S_a

$$S_a = \frac{1}{MN}\sum_{k=1}^{M-1}\sum_{l=0}^{N-1}|z(x_k, y_l| \quad (1)$$

The root mean square, S_q

$$S_q = \sqrt{\frac{1}{MN}\sum_{k=0}^{M-1}\sum_{l=0}^{N-1}(z(x_k, y_l))^2} \quad (2)$$

where M and N are size of the image and $z(x_k, y_l)$ is the height at position (x_k, y_l) from the mean plane.

The peak-valley height, S_y

$$S_y = S_p - S_v \quad (3)$$

where S_p is the highest value and S_v is the lowest value within the scanned area.

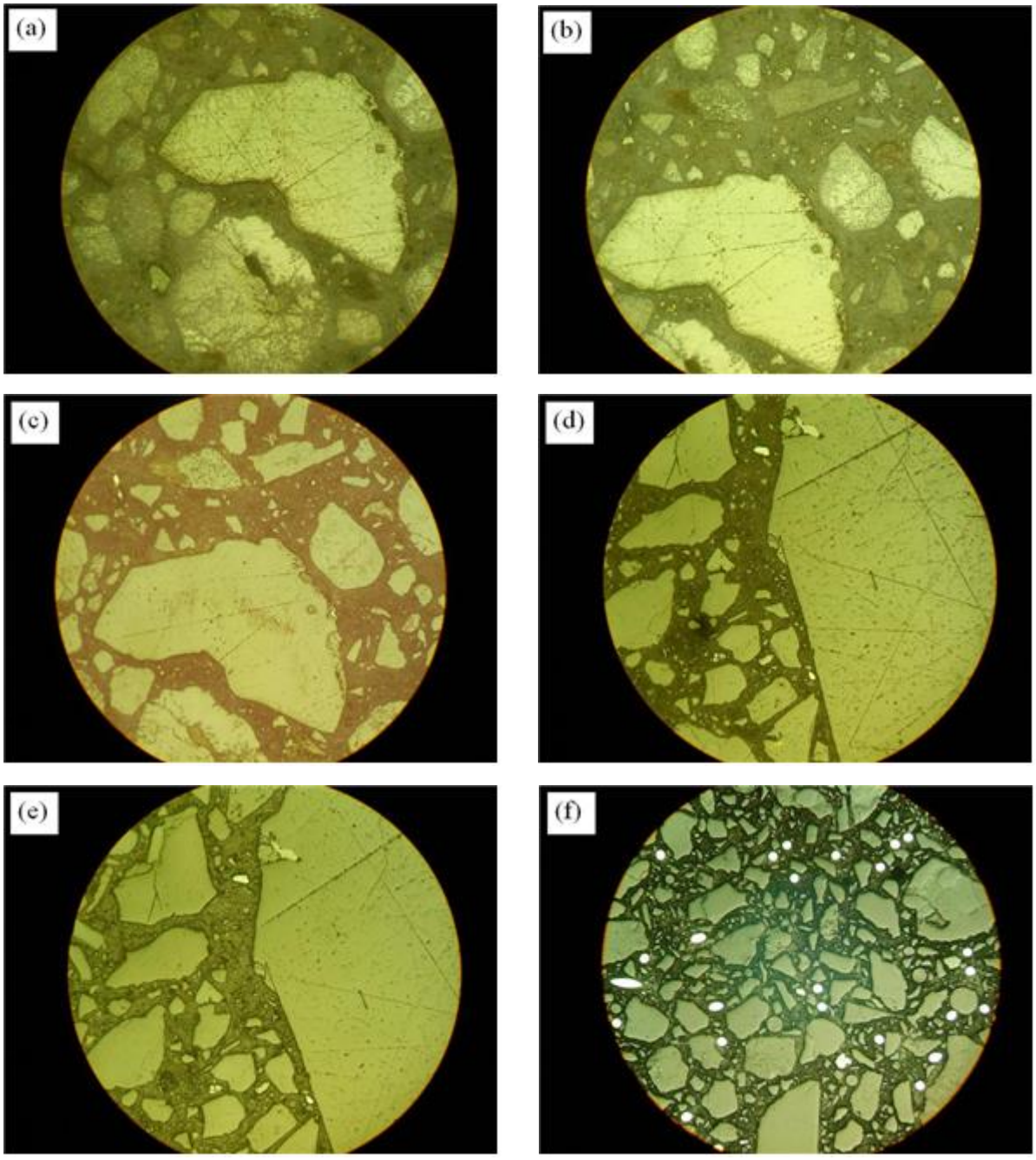

Figure 7. The surface texture of paste and aggregate under a reflected light microscope at x10 x10 magnification after each polishing using (a) MD-Largo (9 μm), (b) MD-Plan (6 μm), (c) MD-Dur (3 μm), (d) MD-Dac (1 μm), and (e) MD-Nap (1/4 μm). (f) The surface texture of the steel fiber-reinforced mortar at x10 x2.5 magnification after MD-Nap (1/4 μm).

2.7. Analysis of backscattered electron image

The Hitachi S-3400N LV-SEM equipped with Oxford INCA software was adopted to take the backscattered electron (BSE) images of the specimen. Before the image acquisition the examined surface of the specimen was sputter-coated with a layer of carbon. The SEM was operated at an accelerating voltage of 5 kV, at a working distance of about 8 mm and in low vacuum condition. The images were taken at a magnification of 500x and were digitized at 2560 x

1920 pixels with a resolution of 0.1 μm/pixel.

The area % of porosity and the area % of unhydrated cement in the ITZ of steel fiber were measured. The upper threshold cut-off value of 45 was set to calculate the area % of porosity. This upper threshold value was determined by visual-checking the colored area on the porosity in the BSE-image during image acquisition. Since the threshold cut-off was performed by the same operator, the accuracy of the upper threshold setting for the porosity was maintained.

In order to perform the calculation of area %, 10-μm wide strips were cut successively from the BSE image using the magnetic lasso tool in Adobe Photoshop software. It started from the edge of steel fiber up to a distance of 60 μm. All strips were then saved at 2560 x 1920 pixels, 8 bit greyscale mode and in jpg format. The features in the strips were segmented manually and measured in area fraction using analySIS®.

2.8. Nanoindentation

A Hysitron Triboindenter with a Berkovich indenter, which is a three-sided pyramid diamond, was used to indent on the cement hydrates in the ITZ between steel fiber and bulk paste. A maximum load of 5 mN was applied. The loading started when the indenter came into the contact with the specimen surface. The indenter stopped penetrating further into the specimen when the pre-specified maximum load was reached. The indenter would then be held for 2 s before unloading. The load increased and decreased at the constant rate of 1 mN/s. The protocol for the movement from one indent to the next was set as a Constant Direction Mode and the distance between two adjacent indents was 10 μm. A typical indentation load versus indentation displacement with the elastic modulus E and the hardness H of a sample can be calculated as follows [14],

$$S = \frac{dP}{dh} = \frac{2}{\sqrt{\pi}} E_r \sqrt{A} \tag{4}$$

$$E = (1 - v^2)\left[\frac{1}{E_r} - \frac{(1-v_i^2)}{E_i}\right]^2 \tag{5}$$

$$H = \frac{P_{max}}{A} \tag{6}$$

Where S is the initial unloading stiffness, P is the indentation load, h is the indentation depth, E_r is the reduced elastic modulus, A is the projected area of the elastic contact, v is Poisson's ratio for the sample, E_i and v_i are Young's modulus and Poisson's ratio for the indenter and P_{max} is the peak indentation load. In our study, the elastic modulus E_i and the Poisson's ratio v_i of the adopted indenter are 1,140 GPa and 0.07, respectively.

3. Results and discussion

3.1. Surface roughness

Figure 8 shows the topography of the epoxy-impregnated paste, steel fiber-ITZ and aggregate-ITZ in the area of 70 x 70 μm. Due to the different hardness of each phase, aggregate and steel fiber were projected out from the paste after polishing. From the 3D view of steel fiber-ITZ and aggregate-ITZ, see Figure 8(b) and (c), the height between the part of steel fiber or aggregate that projected out and the top peak of cement hydrates were around 0.56 μm or 0.70 μm, respectively. It happened only if a pore existed at the edge of the steel fiber or aggregate.

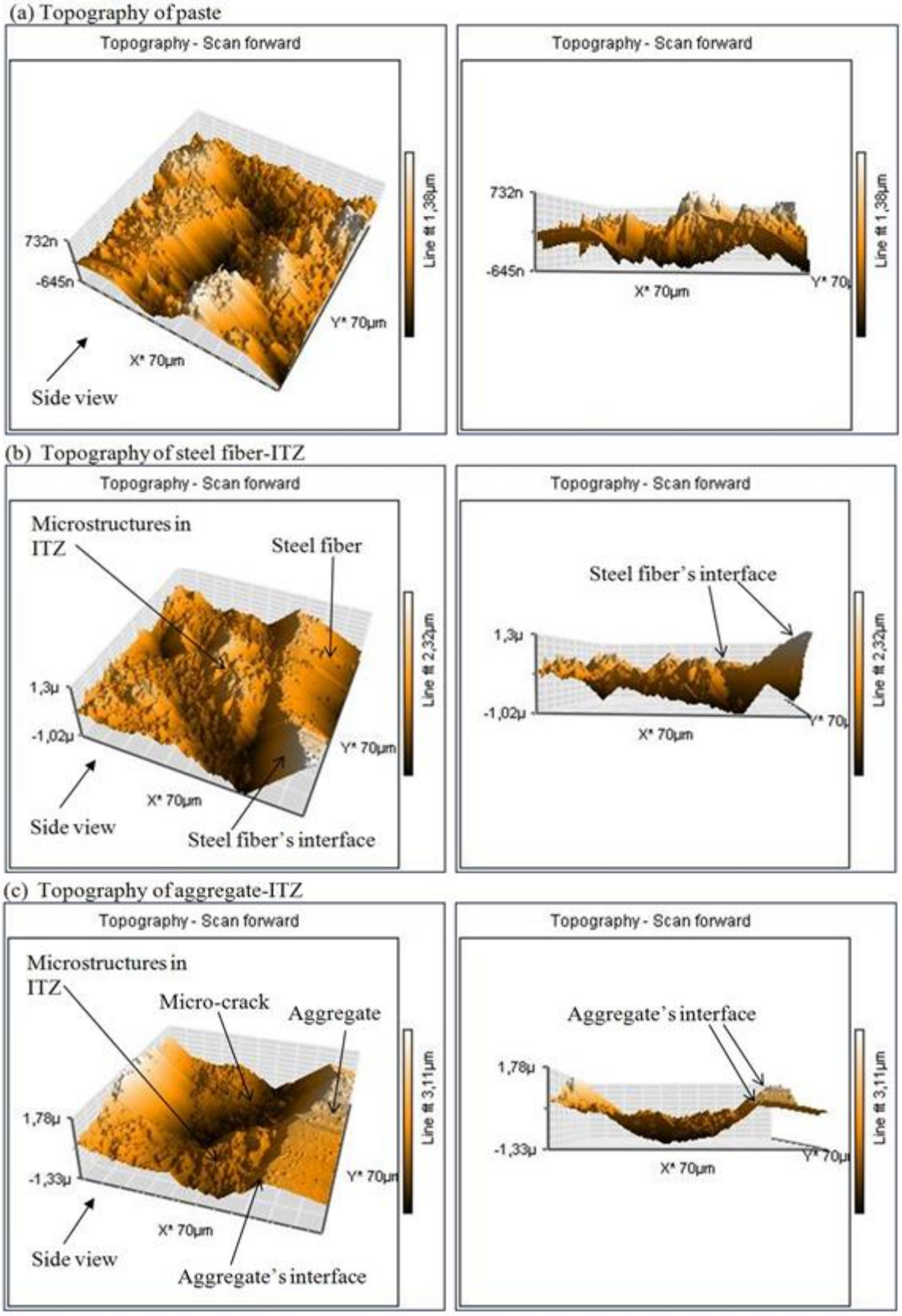

Figure 8. The topography of epoxy-impregnated paste, steel fiber-ITZ and aggregate-ITZ after final polishing - the left image is 3D view and its corresponding side view is shown on the right image.

The roughness average (S_a), the root mean square (S_q) and the peak-valley height (S_y) of the surface of steel fiber, steel fiber-ITZ, bulk paste and aggregate in three different steel fiber-reinforced mortars were measured and are shown in Table 3. The data showed that the average surface roughness of less than 1 μm was achieved on these four phases found in the steel fiber-reinforced mortar. The peak-valley height (S_y) refers to the difference between the highest value and the lowest value found in the scanned area. For steel fiber and aggregate, S_y was less than 1 μm, indicating a good surface roughness had been achieved. For steel fiber-ITZ and bulk paste, S_y was between 2 and 3.5 μm, more than 1 μm. This did not indicate that the sample preparation mentioned in this paper was not good. This was merely due to the porous nature of cement paste. In some region, the epoxy might not vacuum impregnate into the pores properly due to their sizes that were very small. Although this was the case, in overall, the grinding and polishing procedure proposed in this paper yielded a very good flat-polished surface for the study of backscattered electron image analysis and nanoindentation.

Table 3: The roughness average (S_a), the root mean square (S_q) and the peak-valley height (S_y) on the surface of steel fiber, steel fiber-ITZ, bulk paste and aggregate of three different steel fiber-reinforced mortars.

		steel fiber	steel fiber-ITZ	bulk paste	aggregate
w/b 0.3, 0% silica fume, 0.3 vol% steel fiber	S_a (nm)	6.4319	467.86	326.43	16.49
	S_q (nm)	13.695	566.52	403.31	33.15
	S_y (nm)	464.8	3366.83	2649	972.79
w/b 0.3, 10% silica fume, 0.3 vol% steel fiber	S_a (nm)	10.803	339.63	364.34	23.786
	S_q (nm)	21.063	448.52	433.96	35.776
	S_y (nm)	589.92	3431.3	2615.1	485.24
w/b 0.5, 0% silica fume, 0.3 vol% steel fiber	S_a (nm)	23.294	372.5	362.08	19.971
	S_q (nm)	39.229	439.173	440.07	35.661
	S_y (nm)	807.975	2609.23	2555.45	659.81

3.2. Artifacts and countermeasures

The whole grinding and polishing process presented in this study took a total time of 15 minutes when the discs were completely new. However, the total time became longer when the grinding discs and the polishing cloths were getting old. Although each grinding and polishing step is done in two minutes, artifacts such as scratches, edge retention, relief and contamination, as shown in Figure 9, will occur on the specimen surface. Therefore, certain countermeasures should be taken into account during grinding and polishing to prevent those artifacts. They are stated as below:

1) It is advisable that for each grinding or polishing using the force given in Table 2, the duration of more than 3 minutes should be avoided. This is because debris that is detached from the mortar during polishing and grit may accumulate on the discs and then scratch the examined surface. It is important to reduce relief and thermal damage on the examined surface by keeping the grinding and polishing duration short.

2) During the grinding using MD-Piano 220 (68 μm), MD-Piano 600 (30 μm), MD-Piano 1200 (14 μm), water was used to wash away big chunks of debris produced during grinding. This is to avoid the big chunks of debris from scratching the surface of the specimen. It has been reported that water has a tendency to dissolve calcium hydroxide (CH). Wang et al. [15] revealed that the dissolution rate of CH increased exponentially over the pH range of 6.5 to 3. The pH of pure water

is close to 7. Each grinding only lasts for 2 minutes. Therefore, it is assumed that the dissolution of CH should not be too serious in this study. After all, all the specimens are subjected to the same condition in this study. If there is leaching of CH during grinding using water, all the specimens will encounter the same effect. It is very costly if ethanol is used to wash away the big chuncks of debris during grinding.

3) A proper controlled concentration of diamond grit and lubricant should be injected during polishing. Scratches due to the grit are commonly seen when too little lubricant is present in the concentration, see Figure 9(a) and 9(b). Shaking bottle well before polishing helps to distribute evenly diamond grit in the lubricant.

4) Ethanol is used as lubricant during polishing and also for ultrasonically cleaning specimens after each polishing to avoid dissolving CH from the paste. However, epoxy is soluble in ethanol [16]. Ultrasonically treatment of specimens too long in ethanol or too much polishing on the same specimen in a short time will soften the mounting epoxy.

5) Grinding discs and polishing cloths should be ultrasonically washed in the water after use. Cement paste could accumulate on the disc, see Figure 10. This could cause scratches and contamination on the examined surface as shown Figure 9(b). Although the scratches and contamination on the examined surface can be removed by repeating the step, it in fact causes extra work.

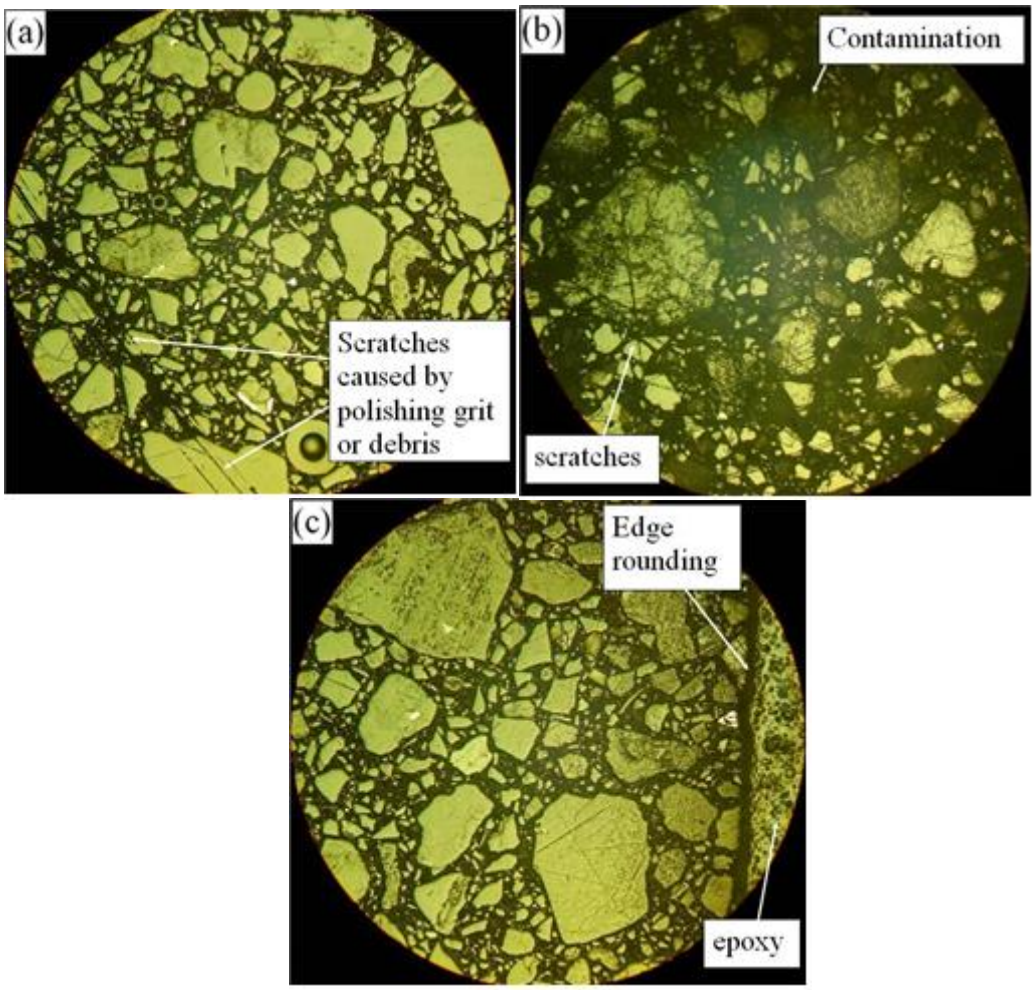

Figure 9. Images taken at x10 x2.5 magnification under a reflected light microscope. (a) Scratches occurred after 1 μm diamond grit polishing. (b) Scratches and contamination after 9 μm diamond grit polishing (c) Edge rounding on the left side of image.

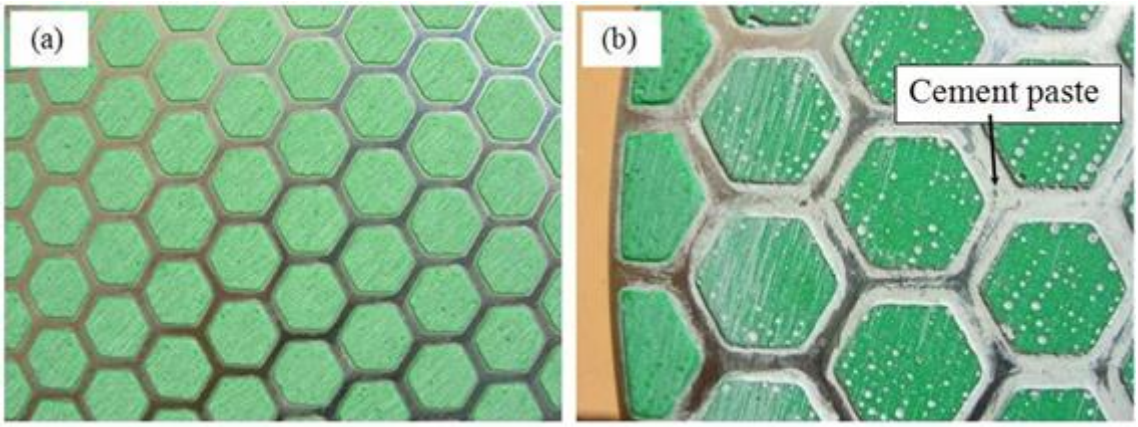

Figure 10. (a) A new MD-Largo disc, and (b) an old MD-Largo disc with the contamination of cement paste.

3.3. Area % of porosity and unhydrated cement in ITZ

The area % of porosity and unhydrated cement versus the distance from the edge of the steel fiber is shown in Fig. 11 with (T) refers to the top and (B) refers to the bottom side of steel fiber that lays in horizontal or in 90 degree angle to the direction of the fresh mortar being poured into the steel mould. The purpose of dividing the steel fiber into two halves (the top side and the bottom side) was to see if any water accumulated at the bottom side of the steel fiber during setting. From the curves shown in Fig. 11, it could be seen that no water accumulated at the bottom side of the steel fiber during setting. If there was, then the area % of porosity at the bottom side would be higher than that at the top side of the steel fiber.

Figure 11 shows that steel fiber-reinforced mortar at w/b 0.3 has a lower area % of porosity than that at w/b 0.5. Regardless of w/b, it can be seen from Figure 11 that the area % of porosity was high at the distance of 10 μm from the edge of the steel fiber. The curve reduced and reached a plateau after the distance of 30 μm away from the steel fiber, indicating that the thickness of the ITZ of steel fiber with diameter 0.16 mm was around 30 μm. An increase in the trend of porosity at the distance 50 μm away from the steel fiber was mainly caused by the presence of the ITZ of neighbouring aggregate.

For unhydrated cement, steel fiber-reinforced mortar at w/b 0.5 with 0% silica fume and that at w/b 0.3 with 10% silica fume showed a low and constant value of area %; while that at w/b 0.3 with 0% silica fume showed an increase at the distance of 20 or 30 μm from the edge of the steel fiber, see Figure 11(b). A low area % of unhydrated cement found near the edge of the steel fiber for the mortar at w/b 0.3 was mainly caused by a locally high w/b formed near the surface of the steel fiber. For steel fiber-reinforced mortar at w/b 0.5, a locally high w/b was believed forming at the surface of steel fiber compared to the matrix. However, due to the high water content in w/b 0.5, almost all the cement grains were hydrated, and thus a low and constant area % of unhydrated cement was observed both in the ITZ and bulk paste.

Figure 11 shows that 10% silica fume does not reduce the area % of porosity by densifying the ITZ between steel fiber and bulk paste. Caliskan [17] shows that only the replacement of cement with 20% silica fume could improve the interfacial bond strength by densifying the cement paste in the ITZ and produced thinner ITZ. On the other hand, silica fume also has a significant influence in increasing the shrinkage compared to plain mortar [18]. The microcracks found in our mortars with 10% silica fume could be due to the high autogeneous shrinkage during setting. The software adopted did not allow the microcracks to be separated from the image analysis. These microcracks were interpreted as pores in the image analysis, and thus a higher area % of porosity was shown in

some areas in mortars with 10% silica fume.

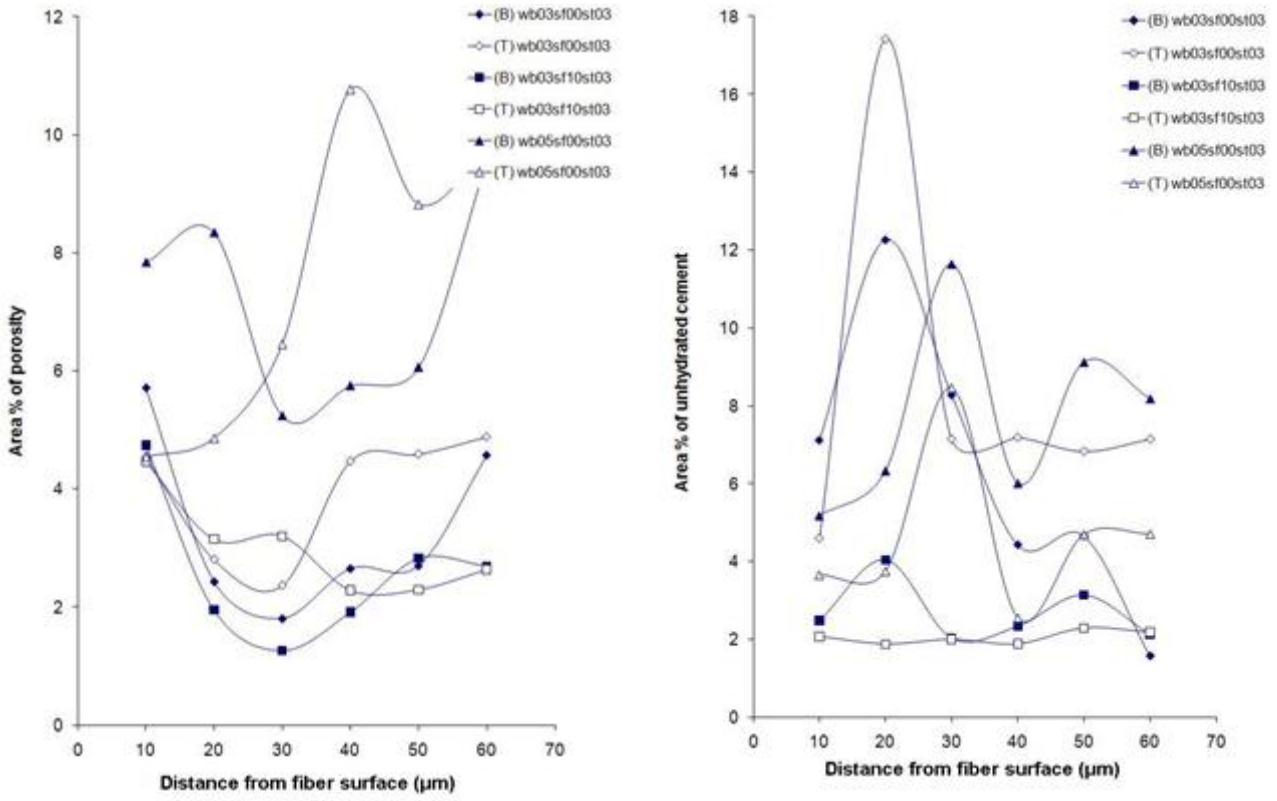

Figure 11. The area % of porosity and unhydrated cement in the ITZ between steel fiber and bulk paste. wb = water/binder, sf = silica fume, st = steel fiber, with two digits after sf and st refer to quantity in % and vol%, respectively.

3.4. Hardness and modulus of cement paste in ITZ

Figure 12 shows the hardness and the modulus profiles of the steel fiber-ITZ-matrix of mortars at (a) w/b 0.3 with 0% silica fume, (b) w/b 0.3 with 10% silica fume, and (c) w/b 0.5 with 0% silica fume. In Figure 12, the vertical axis refers to the edge of the steel fiber and the horizontal axis refers to the distance from the edge of the steel fiber. In this study, the investigation of the nano-mechanical properties of each constituent of cement hydrates was not the main concern. The hardness and the modulus profiles of paste in the ITZ were studied in order to find out how well the bond was formed between the paste and the steel fiber. Therefore, a comparison was made between the hardness profiles found in this study with the hardness profile described by Igarashi et al. [19], as shown in Figure 13. The hardness of paste in the ITZ of steel fiber was between 0.15 and 2 GPa for three different steel fiber-reinforced mortars in this study. This value was reasonable whencompared to the hardness of each constituent of cement hydrates from other literature, see Table 4.

For the mortar at w/b 0.3 with 0% silica fume, the hardness profile shows an obvious increase in the distance 5-35 μm away from the steel fiber's edge. In the 35-65 μm zones, the nanomechanical properties become relatively constant and a plateau is reached. This hardness profiles had similarity with the trend of type I in Figure 13. Therefore, this reflected that the bond between the paste and the steel fiber was quite efficient for mortar at w/b 0.3 with 0% silica fume.

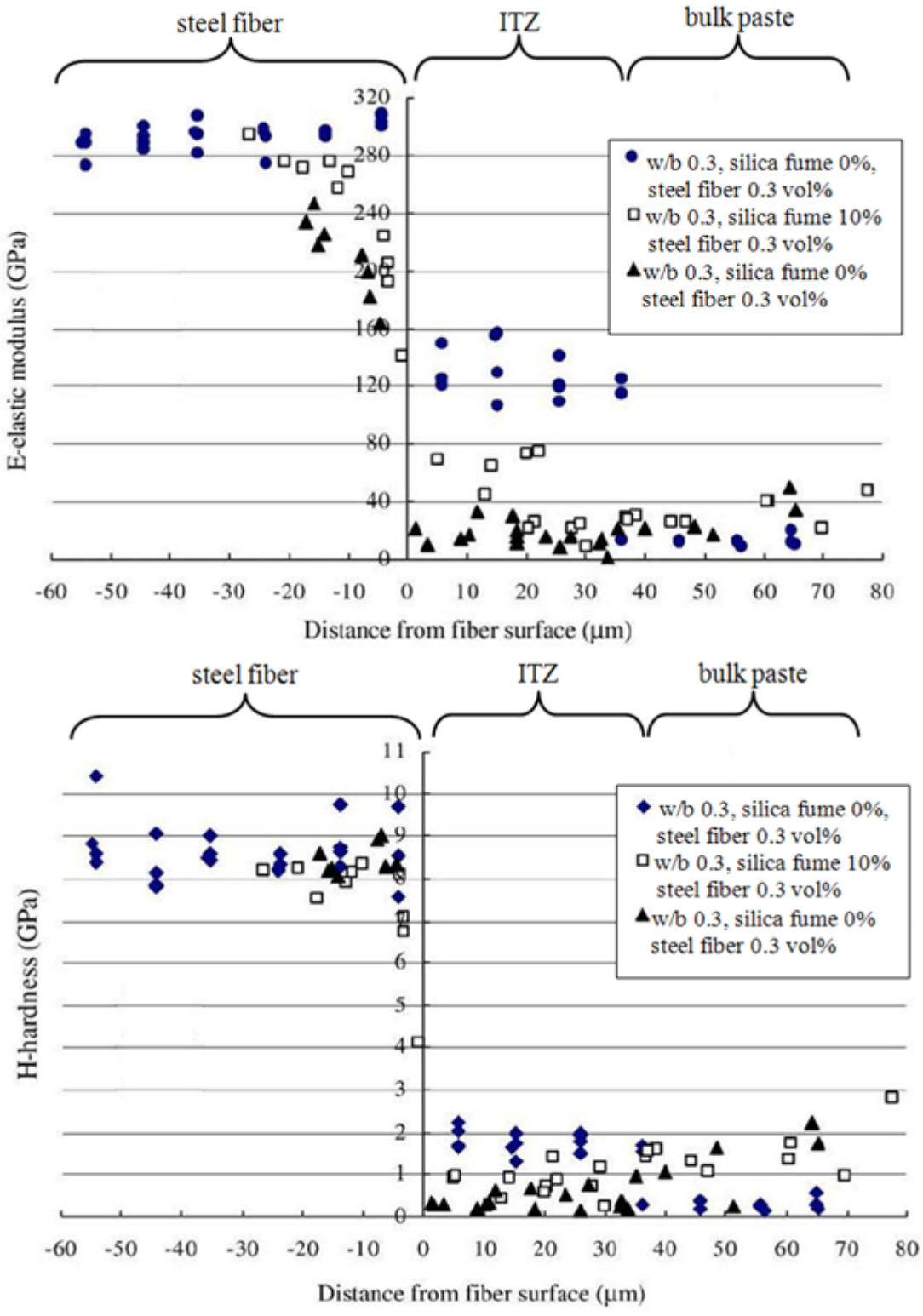

Figure 12. Elastic modulus and hardness profile of ITZ between steel fiber and matrix for 0.3 vol% steel fiber-reinforced mortars with (a) w/b 0.3 with 0% silica fume, (b) w/b 0.3 with 10% silica fume, and (c) w/b 0.5 with 0% silica fume.

For the mortar at w/b 0.3 with 10% silica fume, a relatively low hardness is observed just in the 10-30 μm zones and the hardness profile became relatively constant beyond this zone. It was more like

the trend of type III in Fig. 13. It could be said that for the mortar at w/b 0.3, the bond between the cement paste and the steel fiber for that with 10% silica fume is good, but not as efficient as that with 0% silica fume.

For the mortar at w/b 0.5 with 0% silica fume, the hardness profile of the ITZ was relatively low when it was compared with the mortar at w/b 0.3. The hardness profile was like the trend of type IV, with the lowest hardness was observed near the edge of the steel fiber. This indicates that the interfacial bonding in the mortar at w/b 0.5 was poor and not as effective as that obtained in the mortar at w/b 0.3.

The elastic's modulus of the paste in the ITZ for steel fiber-reinforced mortar at w/b 0.3 with 0% silica fume was around 100 to 160 GPa. This value was similar to the value of each constituent of unhydrated cement shown by other literature, see Table 5. The backscattered electron image analysis in Section 3.3 also revealed the same fact that steel fiber-reinforced mortar at w/b 0.3 with 0% silica fume had higher area % of unhydrated cement in the ITZ of steel fiber compared to the other two mortars. The value of elastic modulus that was between 40 and 80 GPa shown in Fig. 12 could possibly be caused by partial indenting on the unhydrated cement and cement hydrates.

Table 4: Hardness of tricalcium silicate (C_3S), dicalcium silicate (C_2S), tricalcium aluminate (C_3A), calcium aluminoferrite (C_4AF), calcium hydroxide (CH), high density calcium-silicate-hydrate, (C-S-$H_{(HD)}$) and low density calcium-silicate-hydrate (C-S-$H_{(LD)}$) from different literature.

Hardness, H (GPa)								
unhydrated cement				cement hydrates			technique	Ref.
C_3S	C_2S	C_3A	C_4AF	CH	C-S-$H_{(HD)}$	C-S-$H_{(LD)}$		
8.7±0.5	8±1	10.8±0.7	9.5±1.4				nanoindentation	[20]
				1.35±0.5	0.9±0.3	0.8±0.2	nanoindentation	[21]
				1.31±0.23	0.83±0.18	0.45±0.14	nanoindentation	[22]
					1.43±0.29	0.93±0.11	nanoindentation	[5]

Table 5: Elastic's modulus of tricalcium silicate (C_3S), dicalcium silicate (C_2S), tricalcium aluminate (C_3A), calcium aluminoferrite (C_4AF), calcium hydroxide (CH), high density calcium-silicate-hydrate, (C-S-$H_{(HD)}$) and low density calcium-silicate-hydrate (C-S-$H_{(LD)}$) from different literature.

Elastic's modulus, E (GPa)								
unhydrated cement				cement hydrates			technique	Ref.
C_3S	C_2S	C_3A	C_4AF	CH	C-S-$H_{(HD)}$	C-S-$H_{(LD)}$		
135±7	130±20	145±10	125±25				nanoindentation	[20]
147±5	140±10	160±10					resonance frequency	[20]
				38±5	29.4±2.4	21.7±2.2	nanoindentation	[23]
135±7	140±10	160±10		36±3	31±4	20±2	indentation	[21]
				40.3±4.2	29.1±4	18.2±4.2	nanoindentation	[22]
					41.45±1.75	22.89±0.76	nanoindentation	[5]

4. Conclusions

This study reveals that a sample preparation for a cementitious material being able to produce a surface roughness of less than 1 μm with a total time of 15 minutes is very costly and tedious. This condition could only be achieved when the grinding discs and the polishing cloths are new together with a proper control of diamond abrasive and lubricant being injected during polishing. Scratches caused by an accumulated polishing grit or debris detached from the specimen and contamination caused by the polishing cloths are two artifacts that are commonly seen on the specimen. These two artifacts will normally lengthen the time of sample preparation.

This study also reveals that the interfacial transition zone for steel fiber with a diameter of 0.16 mm is found to be around 30 μm. Steel fiber-reinforced mortar at w/b 0.3 with 0% silica fume has the area % of porosity in the ITZ similar to that with 10% silica fume. In fact, at w/b 0.3, steel fiber-reinforced mortar with 0% silica fume has a better bonding at the ITZ compared to that of 10% silica fume. Steel fiber-reinforced mortar at w/b 0.5 with 0% silica fume has less effective bonding compared to that at w/b 0.3 with 0 and 10% silica fume.

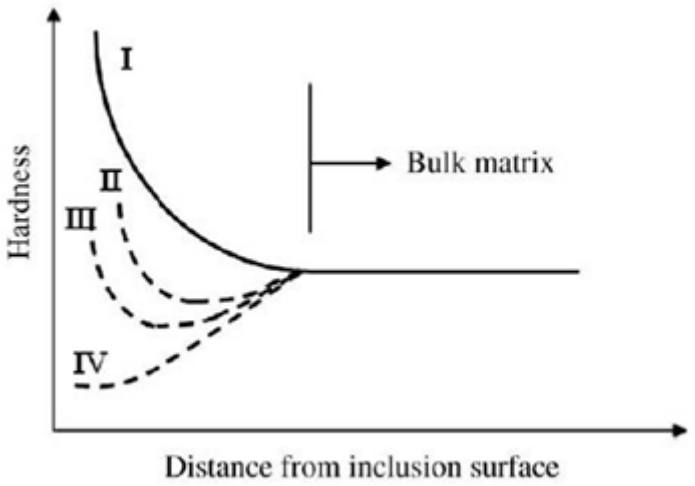

Figure 13. Classification of microhardness profile of cement paste in the interfacial transition zone around a rigid body [19]

Acknowledgments

We thank the funding from the Norwegian Research Council Institution-based Strategic Project (NRC-ISP) on focus area 3 -Sustainable Infrastructure (Grant no 177275). This work also forms a part of NTNU's contribution to the Concrete Innovation Centre (COIN) at Sintef/NTNU, starting in 2007 as a centre for research based innovation (CRI) within concrete technology with 9 industrial partners: Aker Solutions, Norcem Heidelberg, Borregaard, Maxit, Skanska, Rescon Mapei, UNICON, Veidekke and the Norwegain Road directory. Finally, I would like to thank the engineer Arild Monsøy for his friendly discussion and some technical supports.

REFERENCES

[1] Head, M.K., and Buenfeld, N.R. Measurement of aggregate interfacial porosity in complex, multi-phase aggregate concrete: Binary mask production using backscattered electron, and

energy dispersive X-ray images. Cem Concr Res 2006. 36(2): p. 337–345.

[2] Mouret, M., Ringot, E., and Bascoul, A. *Image analysis: A tool for the characterisation of hydration of cement in concrete - metrological aspects of magnification on measurement*. Cem Concr Compos 2001. 23(2-3): p. 201–206.

[3] Kjellsen, K.O., Monsøy, A., Isachsen, K., and Detwiler, R.J. *Preparation of flat-polished specimens for SEM-Backscattered electron imaging and X-ray microanalysis - importance of epoxy impregnation*. Cem Concr Res 2003. 33(4): p. 611–616.

[4] Wong, H.S., and Buenfeld, N.R. *Patch microstructure in cement-based materials: Fact or artefact?* Cem Concr Res 2006. 36(5): p. 990–997.

[5] Mondal, P., Shah, S.P., and Marks, L. *A reliable technique to determine the local mechanical properties at the nanoscale for cementitious materials*. Cem Concr Res 2007. 37(10): p. 1440–1444.

[6] Miller, M., Bobko, C., Vandamme, M., and Ulm, F-J. *Surface roughness criteria for cement paste nanoindentation*. Cem Concr Res 2008. 38(4): p. 467–476.

[7] Sakulich, A.R., and Li, V.C. *Nanoscale characterization of engineered cementitious composites (ECC)*. Cem Concr Res 2011. 41(2): p. 169–175.

[8] Kenny, S.D., Mulliah, D., Sanz-Navarro, C.F., and Smith, R. Molecular dynamics simulations of nanoindentation and nanotribology. Philos T R Soc A 2005. 363(1833): p. 1949–1959.

[9] Lee, S.F., He, J.Y., Wang, X.H., Zhang, Z., and Jacobsen, S. *Study of p-h curves on nanomechanical propertis of steel fiber reinforced mortar*. In: Bittnar Z, Zeman J, Němeček, Šmilauer V, Bartos PJM (eds), Nanotechnology in Construction 3, Proceedings, Prague, Czech Republic 2009. p. 281-286. Springer Berlin Heidelberg.

[10] ISO-14577-1, Metallic Materials - Instrumented Indentation Test for Hardness and Materials Parameters. Part I: Test Method, Geneva, Switzerland 2002.

[11] Lee, S.F., and Swallowe, G.M. *Direct measurement of high rate stress-strain curves using instrumented falling weight and high-speed photography*. Imaging Sci J 2004. 52(4): p. 193–201.

[12] Lee, S.F., and Swallowe, G.M. *Quasi-static and dynamic compressive behaviour of poly(methyl methacrylate) and polystyrene at temperatures from 293K to 363K*. J Mater Sci 2006. 41(19): p. 6280–6289.

[13] Struers A/S. Struers Metalog Guide -User's manual. Valhøjs Alle 176, DK-2610 Rødovre, Denmark 2000.

[14] Oliver, W.C., and Pharr, G.M. *Improved technique for determining hardness and elastic modulus using load and displacement sensing indentation experiments*. J Mater Res 1992. 7(6): p. 1564–1580.

[15] Wang, J., Keener, T.C., Li, G., and Khang, S-J. *The dissolution rate of $Ca(OH)_2$ in aqueous solutions*. Chem Eng Commun 1998. 169(1): p. 167–184.

[16] Glauert, A.M., Glauert, R.H. *Araldite as an embedding medium for electron microscopy*. J Biophys Biochem Cytol 1958. 4(2): p. 191–194.

[17] Caliskan, S. *Aggregate/mortar interface: Influence of silica fume at the micro- and macro-level*. Cem Concr Compos 2003. 25(4-5): p. 557–564.

[18] Rao, G.A. *Long-term drying shrinkage of mortar - Influence of silica fume and size of fine aggregate*. Cem Concr Res 2001. 31(2): p. 171–175.

[19] Igarashi, S., Bentur, A., and Mindess, S. *Microhardness testing of cementitious materials*. Adv Cem Based Mater 1996. 4(2): p. 48–57.

[20] Velez, K., Maximilien, S., Damidot, D., Fantozzi, G., and Sorrentino, F. *Determination by nanoindentation of elastic modulus and hardness of pure constituents of portland cement clinker*. Cem Concr Res 2001. 31(4): p. 555–561.

[21] Acker, P. *Micromechanical analysis of creep and shrinkage mechanisms. In: Ulm F-J,*

Bazant Z, Wittmann F (eds), Creep, Shrinkage and Durability Mechanics of Concrete and other Quasi-Brittle Materials 2001. Oxford, UK, Elsevier.

[22] Ulm, F-J., and Constantinides, G. *The nanogranular nature of C-S-H*. J Mech Phys Solids 2007. 55(1): p. 64–90.

[23] Constantinides, G., and Ulm, F-J. T*he effect of two types of C-S-H on the elasticity of cement – based materials*: *Results from nanoindentation and micromechanical modeling.* Cem Concr Res, 2004. 34(1): p. 67-80.